Journal of Constructional Steel Research 128 (2017) 371–379

Contents lists available at ScienceDirect

Journal of Constructional Steel Research

# Structural behavior of extreme thick-walled cold-formed square steel columns

Dongyu Liu [b], Hongbo Liu [a,b,c,*], Zhihua Chen [a,b], Xiangwei Liao [b]

[a] State Key Laboratory of Hydraulic Engineering Simulation and Safety, Tianjin University, Tianjin 300072, China
[b] Key Laboratory of Coast Civil Structure Safety of China Ministry of Education, Tianjin University, China
[c] School of Engineering, University of Edinburgh, Edinburgh, EH93FB, UK)

ARTICLE INFO

*Article history:*
Received 23 April 2016
Received in revised form 8 September 2016
Accepted 14 September 2016
Available online xxxx

*Keywords:*
Cold-formed square steel column
Extreme thick-walled
Axial compression bahavior
Experimental research
Numerical simulation
Prediction formula

ABSTRACT

This paper describes a study on the extreme thick-walled cold-formed square columns which are manufactured from circular to square shape, of which the width was 800 mm and the thickness was 22 mm. A systematic investigation of material behavior, residual stress distribution, and axial compression performance was performed numerically and experimentally. Results demonstrate thefollowing.1) The material properties of cold-formed columns manufactured by indirect method are clearly changed because of the cold-formed processes and are more uniform than those of cold-formed columns manufactured by direct method. 2)The extreme thick-walled cold-formed square columns work well under axial compression. 3) The residual stresses at the middle and corner parts of extreme thick-walled cold-formed square columnsareapproximately95 and 210 MPa, respectively.


## 1. Introduction

Cold-formed steel members are widely used in civil engineering because of their high strength-to-weight ratio; their thickness is generally limited to approximately3 mm because of the limitations of cold-forming technology in the early stage. This thickness is much thinner than that of hot-rolled steel section. Nowadays, cold-formed sections with a wall-thickness greater than 6 mm, which are referred to as "thick-walled", are more commonly manufactured and used in civil engineering [1]. They are commonly fabricated as closed shapes, such as circular or square hollow sections, and used increasingly in columns of high-rise buildings. The maximum size for the square hollow section is 800 mm wide by 22 mm thick; this type of section was used in the Tianjin Wanhui Square Project in China.

The cold-formed square hollow sections are divided into two kinds based on the forming processes [2–3]. A cold-formed square hollow section can be formed by rolling an annealed flat strip directly onto a square hollow section, which is then welded at the edges. A cold-formed hollow section can also be formed by first rolling an annealed flat strip onto a circular hollow section, which is then welded at the edges; the process is completed by further rolling onto a square hollow section. In this paper, the former forming process is called "direct square method," and the latter is called "indirect method from circular to square." The different forming processes for cold-formed steel members are known to result in their different mechanical properties, such as yield strength, residual stress distribution, axial compression behavior, and so on.

The material behavior is enhanced by cold-form processing, which make its structural behavior different from the hot-rolled steel members [4–7]. Although many studies have been performed to investigate the mechanical behavior of cold-formed steel members, they were mainly focused on thin-walled cold-formed steel members manufactured by the direct square method [8–13]. These studies provided important data for the design codes of thin-walled cold-formed steel members.

Few studies have analyzed the material properties and strengths of thick-walled cold-formed steel members. Li et al. [14], Li et al. [15], and Hu et al. [5] studied the strain hardening effect experimentally and theoretically for thick-walled cold-formed steel sections with thickness ranging from 8 mm to 12 mm. Guo et al. [1] studied the mechanical behavior of thick-walled cold-formed steel stub columns with thickness ranging from 8 mm to 12 mm under axial loading. Tong et al. [2] studied longitudinal residual stresses for cold-formed thick-walled square hollow sections.

The literature review above shows that past studies only focused on cold-formed thick-walled section, whose cross-section was smaller than 400 mm × 400 mm and whose thickness was thinner than 12 mm. The mechanical behavior of cold-formed thick-walled square

* Corresponding author at: State Key Laboratory of Hydraulic Engineering Simulation and Safety, Tianjin University, Tianjin 300072, China.
*E-mail address:* hbliu@tju.edu.cn (H. Liu).

http://dx.doi.org/10.1016/j.jcsr.2016.09.004
0143-974X/

hollow steel members change significantly with the increase of the cross-section and thickness. Therefore, the present work experimentally and theoretically studies the material properties, structural behavior, and strengths of cold-formed thick-walled steel sections with cross-sections of about 800mm × 800 mm and thickness greater than 22 mm.

## 2. Experimental scheme

### 2.1. Specimens design

Two thick-walled cold-formed steel stub columns with same geometric parameters were designed for this test, as shown in Fig. 1. The specimens were manufactured by indirect method from circular tosquare. The cross-section was 800 mm × 800 mm, the thickness was 22 mm, and the height was 2.4 m.

### 2.2. Material mechanical property

To understand the material mechanical property of the thick-walled cold-formed steel members with different cross-section, a total of 27 tensile coupon tests on three cross-section steel members were performed, as reported in Table 1; the tests included three corner coupons, three near -corner coupons, and three flat coupons from each specimen, as shown in Fig. 2. All these coupons were cut from the longitudinal direction. The geometric size of the coupons from the flat position is shown in Fig. 3(a). The geometric sizes of coupons from the flat corner position and near -corner position are shown in Fig. 3(b). The material properties of the cold-formed steel section for each group were determined as the average value of the three coupon tests from the same position. All the coupon dimensions complied with the Chinese metallic material-tensile testing code [16].

The tensile coupons were tested according to the with the Chinese metallic material-tensile testing code [16] using a 600 kN capacity Universal Testing Machine. The average stress-strain curve for each position is shown in Fig. 4. The average values of yield strength, ultimate strength, yield-strength ratio, and elongation for each position are listed in Table 1. Given that some coupons do not have evident yield platforms, the stress of 0.2% residual deformation was set as the yield strength.

**Fig. 1.** The geometric size of the tested specimen.

**Table 1**
The material test results of the cold-formed members.

| Square tube | Position | Yield strength (MPa) | Ultimate strength (MPa) | Yield ratio | Elongation |
|---|---|---|---|---|---|
| 600 × 16 | Middle | 396 | 475 | 0.834 | 18.50% |
| | Side | 347 | 447 | 0.776 | 28.50% |
| | Corner | 415 | 501 | 0.828 | 19.30% |
| 700 × 20 | Middle | 375 | 450 | 0.833 | 23.50% |
| | Side | 396 | 458 | 0.865 | 20.00% |
| | Corner | 397 | 469 | 0.846 | 22.70% |
| 800 × 22 | Middle | 328 | 434 | 0.756 | 30.00% |
| | Side | 399 | 481 | 0.83 | 24.00% |
| | Corner | 386 | 472 | 0.818 | 25.20% |

Based on the test results shown in Fig. 4–5 and Table 1, the following conclusions were formed:

1) Almost all tensile coupons experience three stages: yielding, necking, and fracture; the fractures of all tensile coupons are always located at the parallel section as shown in Fig. 5. But several coupons had no yielding stages because the cold-formed process reduced the ductility of the steel materials to some extent.
2) Given that the cold-formed steel members formed by indirect method from circular to square experience the cold forming processes two times, its mechanical properties are more uniform than that of cold-formed steel members manufactured by direct method; this was proven by the test results. The yield strengths for the corner parts were 19.6, 5.9, and 17.68% higher than that of other locations, whereas the yield strengths for corner parts for the cold-formed steel members manufactured by direct method in previous studies were 30–50%. Therefore, the cold forming process has a significant effect on the material properties.
3) In addition to the individual tensile coupons, the mechanical properties of the cold-formed steel members studied in this research meet the following requirements: the elongation must be higher than 20%, and the yield ratio must be lower than 0.85.

The yield strengths of the studied cold-formed steel members were calculated by Formula (1) given in "Technical code of cold-formed thin-walled steel structures"(GB 50018-2002) [17]. $f'$ is the calculated strength value of cold-formed steel. $f$ is the design strength value of steel. $\eta$ is the coefficent which depends on the shaping method, at this time, the square columns are manufactured from circular columns, so $\eta = 1.7$[17]. $\gamma$ is the ratio of tensile strength to yield strength, regarding Q235 steel, $\gamma = 1.58$.n is the number of corners of cross section, for the columns here, $n = 4$.$\theta_i$ is the central angle of corner which is defined with rad. $l$ is the length of cross section central axial line. $t$ is the thickness of column section. The calculation results are listed in Table 2.

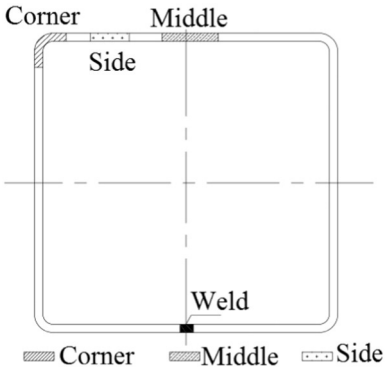


**Fig. 2.** Specimen sampling position.

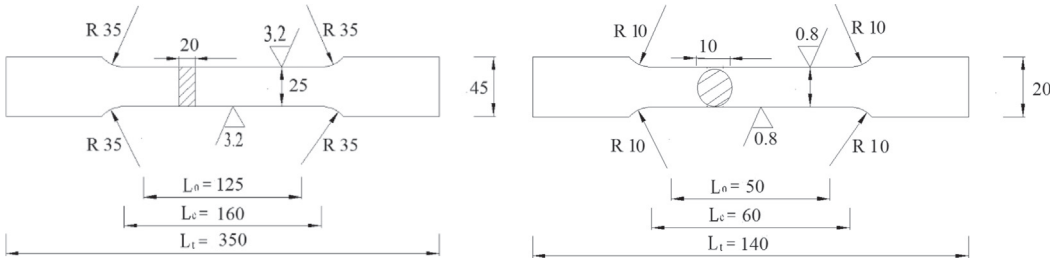


(a) Side & Middle specimen dimensions (b) Corner part specimen dimensions

**Fig. 3.** The form and dimensions of specimens (Unit: mm).

The ratio of the calculated value to the test value is about 0.8 on average. Therefore, Formula (1) is able to predict the yield strength of the thick-walled cold-formed steel members manufactured by indirect method.

$$f' = \left[1 + \frac{\eta(12\gamma - 10)}{l} \sum_{i=1}^{n} t \frac{\theta_i}{2\pi}\right] f \tag{1}$$

### 2.3. Test conditions and procedures

In the test, an electro hydraulic servo pressure machine was used to control pressure and displacement well. The vertical deformation and lateral deformation in the middle of the column were measured by a displacement meter. The strain gauges were located at 1/4, 1/2, and 3/4 of the column height, as shown in Fig. 6. The overall view is shown in Fig. 7.

In the test, 2000 kN weight (approximately 10% of ultimate load) was applied for 10 min as the pre-loading process to ensure that every part contacts well, and the test signal transmission works well. The loading process maintained a smooth loading rate. It was controlled according to the pressure first. Then, it was controlled by displacement at a load of about 15,000 kN. The ultimate load was determined according to the following codes: the displacement increases as load drops rapidly, or the specimen crash.

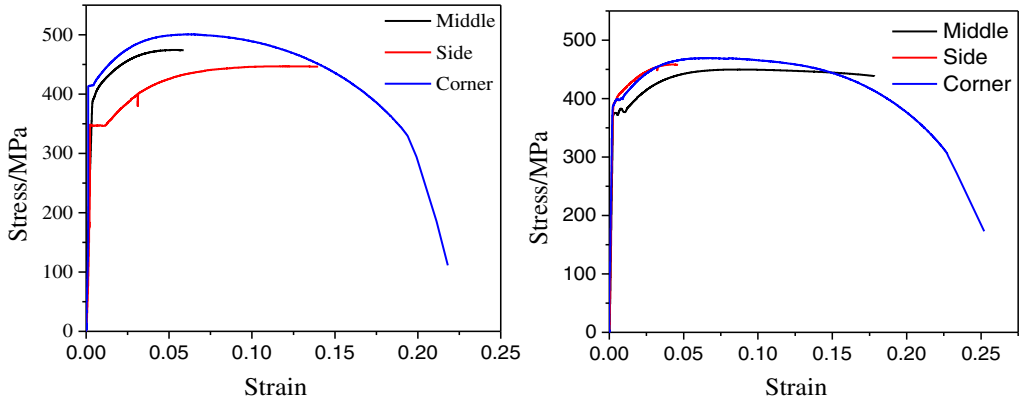


(a) Specimens from square tube 600mm×16mm (b) Specimens from square tube 700mm×20mm

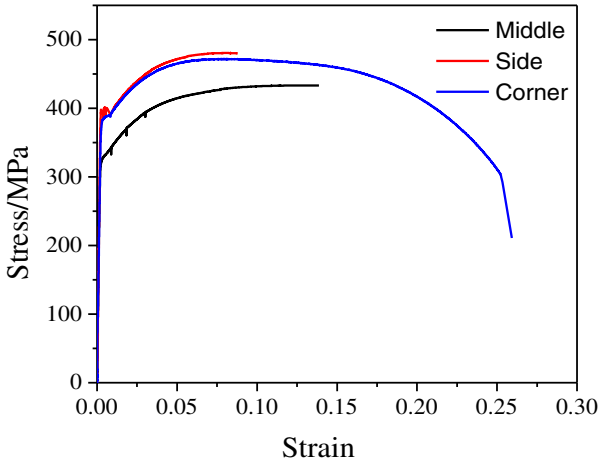


(c) Specimens from square tube 800mm×22mm

**Fig. 4.** Stress-strain curve from tensile coupon test.

(a)Middle part specimens (b)Side part specimens (c)Corner part specimens

**Fig. 5.** The specimen fractured morphology

## 3. Experimental results analysis

The first specimen reached ultimate load at 21,800 kN; at the same time, concave-convex deformation was present at adjacent surfaces of the upper region. The second specimen reached ultimate load at 22,000 kN and had no evident phenomenon. Finally, the maximum deformation of Specimen 800-22-1 and Specimen 800-22-2 were 24.79 mm and 20.41 mm, respectively. The failure modes are shown in Fig. 8.

The load-strain curves for the typical measured points are shown in Figs. 9 and 10. The load-strain curves of measuring points 1, 11, 21, and 31 at the corner part and measuring points 5, 17, 25, and 37 at the middle flat part are shown in Fig. 9 to compare the strain variation trend between these two parts. The annular curve in Fig. 9 (a) is a result of exchanging the loading regime; point 31 of column 800-22-1 was broken soon after the start of the experiment, so its curve wasn't plotted. The strain of 800-22-1 is smaller than that of 800-22-2, when the ultimate load is reached. After observing all the selected points, the elastic developments of both the specimens are not clear. More importantly, the strains at the corner are similar to the strains at the flat part, even though the initial residual strains of these two parts are different. The load-strain curves of measuring points 23, 25, and 27 are plotted in Fig. 10 to analyze the strain distribution along the longitudinal direction. The strains have no obvious change along the longitudinal direction.

**Table 2**
Comparison between test value and calculation value for yield strength.

| Section | Position | Yield strength $f_y$ (MPa) | Calculated strength $f_1$ (MPa) | Calculated bearing capacity column (kN) | Strength ratio $f_1/f_y$ |
|---|---|---|---|---|---|
| 600 × 16 | Middle | 396 | 302.33 | 11,300 | 0.763 |
| | Side | 347 | | | 0.871 |
| | Corner | 415 | | | 0.729 |
| 700 × 20 | Middle | 375 | 294.216 | 16,000 | 0.785 |
| | Side | 396 | | | 0.743 |
| | Corner | 397 | | | 0.741 |
| 800 × 22 | Middle | 328 | 290.87 | 19,900 | 0.887 |
| | Side | 399 | | | 0.729 |
| | Corner | 386 | | | 0.754 |

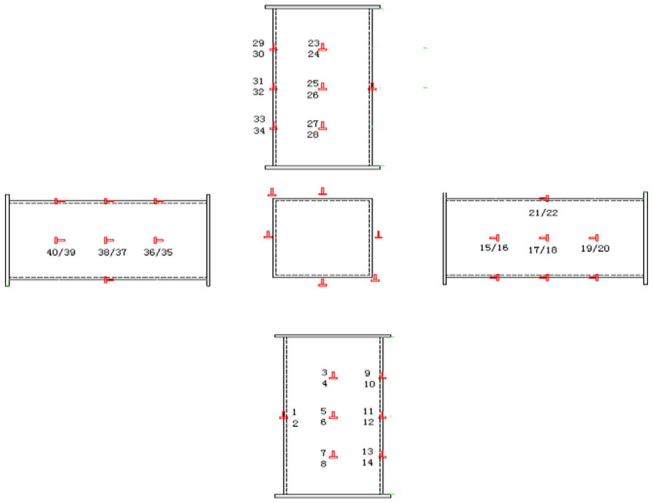


**Fig. 6.** The location of strain gauges.

## 4. Numerical simulation

### 4.1. Axial compression performance simulation

ABAQUS software was used to predict the stress and deformation of thick-walled cold-formed steel stub columns under axial compression and to analyze the residual stress distribution induced by the forming process.

The procedures to predict the axial compression behavior of steel columns is listed as follow. Step 1: Establish the finite element model; Step 2: Run eigenvalue buckling analysis to obtain the worst initial imperfection distribution; Step 3: Run nonlinear analysis to obtain ultimate loads and critical displacement considering the material nonlinearity and geometric nonlinearity.

The rectangle shell element S4R was adopted to simulate the steel stub column. The thickness of the shell element S4R was set as 22 mm. The size of the mesh was controlled at about 50 mm, and the mesh size in the corner of the column was set to about 25 mm to ensure simulation accuracy.

**Fig. 7.** The axial compression test equipment.


(a)800-22-1 (b)The concave surface of 800-22-1 (c)800-22-2

**Fig. 8.** Post -test phenomenon.

The FE model for the thick-walled cold-formed steel column was divided into two parts based on material property. One was the side and corner parts which have similar material properties, and the other was the middle flat part, as shown in Fig. 11 and Fig. 12. The material mechanical property in the yellow section of the FE model was set with yield strength at 386 MPa, ultimate strength at 472 MPa, and elastic modulus at 210 GPa. The material mechanical property in the blue section of the FE model was set with yield strength at 328 MPa, ultimate strength at 434 MPa, and elastic modulus at 210 GPa, the ultimate strains of two kinds of material were both defined as 0.1,the material properties used in this FE model are shown in Fig. 13.

Eigenvalue buckling analysis was first performed to obtain the elastic critical buckling load, as well as the failure modes for the nonlinear analyses at a later step. The deformation was enlarged 240 times to observe the deformation well as shown in Fig. 14. The elastic critical buckling load was 41,800 kN.

Nonlinear analysis was then performed to obtain the nonlinear critical load, first initial imperfection was imposed on the structure, and then considering both materials nonlinearity and geometric nonlinearity, displacement was imposed on a reference point which had been coupled with the top surface of the column to get the ultimate load. Nonlinear critical load was 19,810 kN. Fig. 15 shows the von-Mises

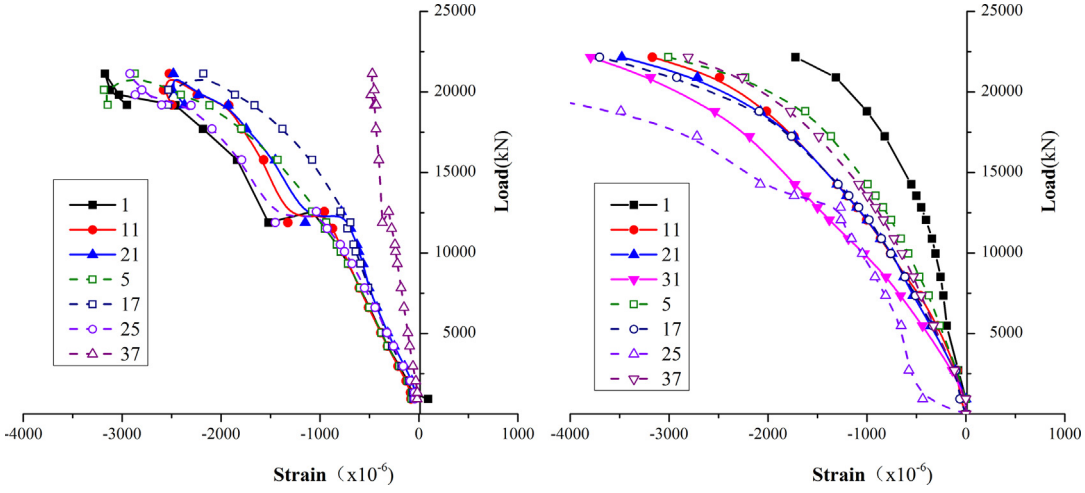


(a)800 -22 -1 (b)800-22 -2

**Fig. 9.** Load-strain curve of middle section.

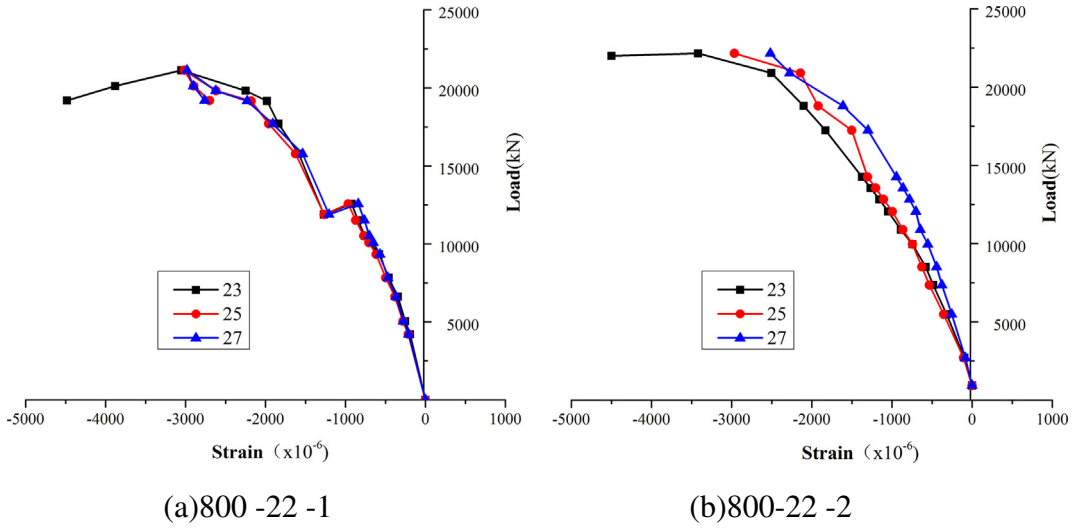


**Fig. 10.** Load-strain curve of the longitudinal direction.

stress distribution when nonlinear critical load is reached, and the deformation in Fig. 15 had been magnified for 3 times. It can be found from Fig. 15 that the simulated deformation pattern is very similar to the actual pattern with the convex-concave phenomenon.

The load-displacement curves were shown in Fig. 16. The average ultimate compression load of steel square column with section 800 mm × 22 mm from test was 21,640 kN, and corresponding value from numerical simulation was 19,810 kN, which was consistent with the test data. However, there was remarkable difference about the displacement as shown in Fig. 16, and the difference may result from following conditions: 1) the test measuring error; 2) difference of initial imperfections (e.g. initial geometric imperfection, residual stress induced by cold-form process, stress-strain model of materials and so on) between the numerical model and the tested specimens.

### *4.2. Forming process simulation*

Cold-formed tubes with size of 600 mm × 20 mm to 800 mm × 25 mm were first processed into a circular tube. Then, the tubes were squeezed into square sections. The specific process was as follows: push the circular pipe, and hydraulic pushing, lateral and extrusion, and adjusting shape, online nondestructive detection and correction adjustable straight, sawing and aging treatment.

The forming process of square members with a dimension of 800 mm × 22 mm and a height of 2400 mm was analyzed in ABAQUS in the same way as the axial compression simulation. The input material property parameter values of yield strength, ultimate strength, elastic modulus, and the Poisson's ratio were 328 MPa, 434 MPa, 210 GPa, and 0.3 respectively, the ultimate strain was defined as 0.1, which is

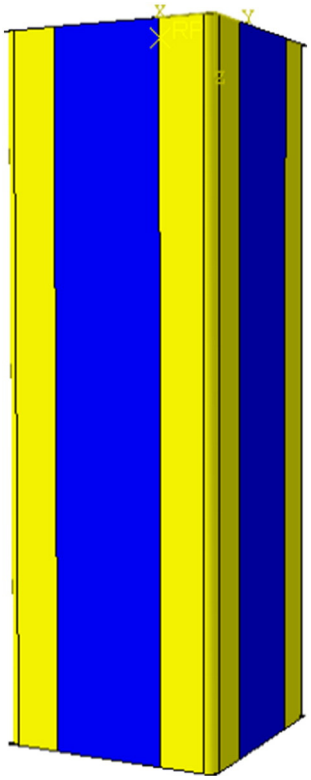

**Fig. 11.** Section partition.

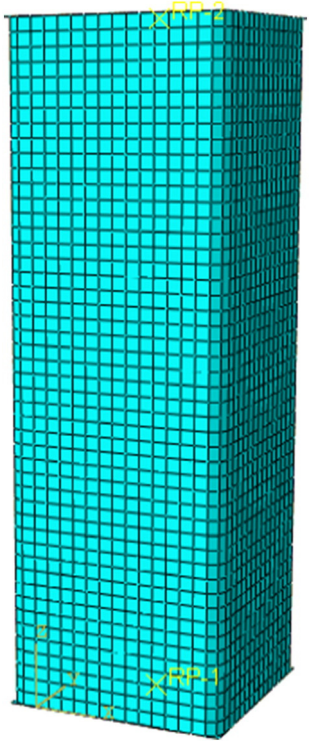


**Fig. 12.** Mesh partition.

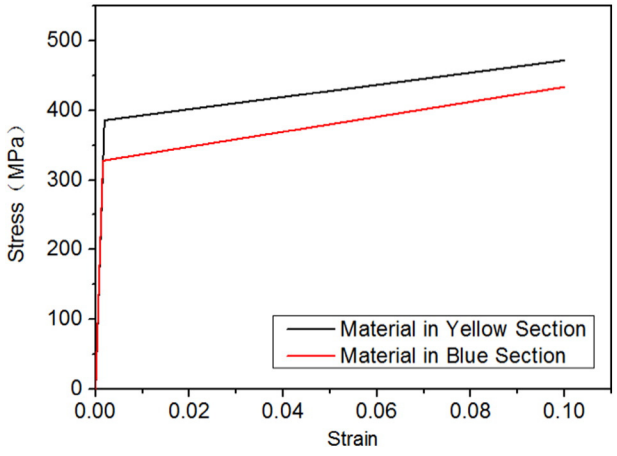


**Fig. 13.** Stress-strain curves used in FE model.

the same as the material used in blue section above. First, a circular tube model was established according to the actual shape shown in Fig. 17; the grid mesh was similar to the mesh discussed in Section 4.1. The forming process was simulated by the contact modular of ABAQUS. The von-Mises stress of the forming process is shown in Fig. 18, and the post-formed von-Mises stress is shown in Fig. 19.

As clearly illustrated in Figs. 18–20, the stresses at the corner were larger than those in the middle part. Given the steel hardening effect, the material yield strength is therefore larger, whereas the strength of the middle plate is basically the same as the raw material. After the forming process, part of the stress is reduced as a result of the elastic strain's recovery; the residual stresses at the middle part and the corner part were about 95 MPa and 210 MPa, respectively, or about $0.3f_y$ and $0.6f_y$, respectively. The section stress distribution is shown in Fig. 20.

## 5. Parameter analysis and calculation formula of axial compression capacity

The different sections and different slenderness ratios of the columns is also examined. Similar to the model shown in Section 4.1, models with sections of 600 × 16 and 700 × 20 were established to investigate the influence of different section sizes. New models with the

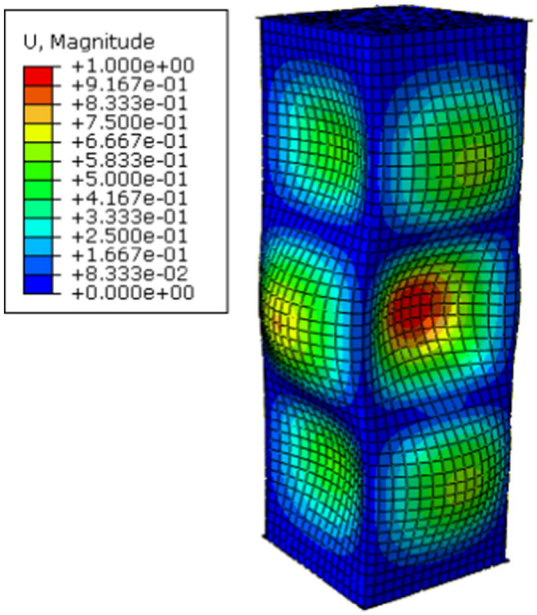


**Fig. 14.** First order buckling mode (cm).

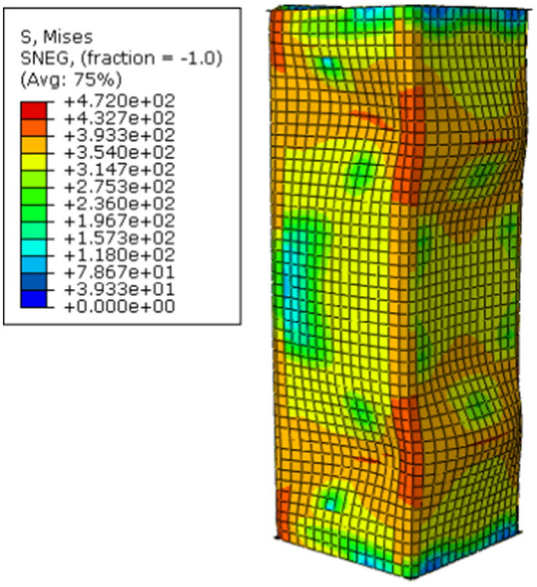


**Fig. 15.** Von-Mises stress distribution (MPa).

heights of 4.8 m and 8 m were established to discover the influence of different slenderness ratios. The numerical axial displacement was found to be inaccurate. Thus, the present study only concentrated on the bearing capacity of these columns.

A formula for calculating the design load for thin-walled compression members is proposed based on the Chinese code (50,018–2002 GB) [17]:

$$\frac{N}{\phi A_e} \le f \tag{2}$$

$$f = \frac{f_m A_m + f_c A_c}{A_e} \tag{3}$$

In the formula, $f$ is the design strength value of steel, and determined by formula (3); $A_e$ is the effective section; and $\varphi$ is the stability coefficient which is relevant with slenderness ratio$\lambda$, and determined by Chinese code [17]; $f_m$and $f_c$ are the yield strength of middle part and corner part of square steel columns, which were list in Table 1; $A_m$and $A_c$ are the cross area of the middle part and corner part, which were shown in Fig. 12.

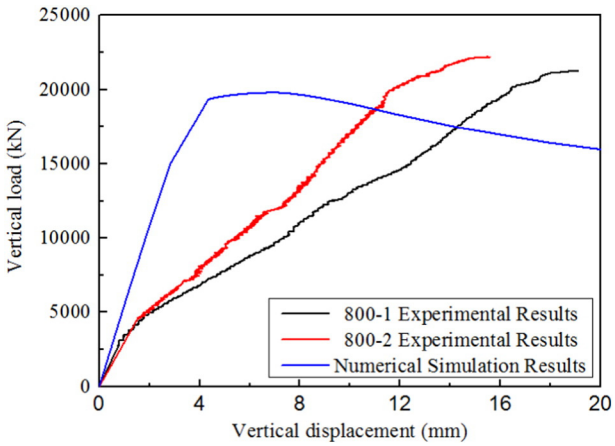


**Fig. 16.** Load-displacement curves for the testes steel columns.

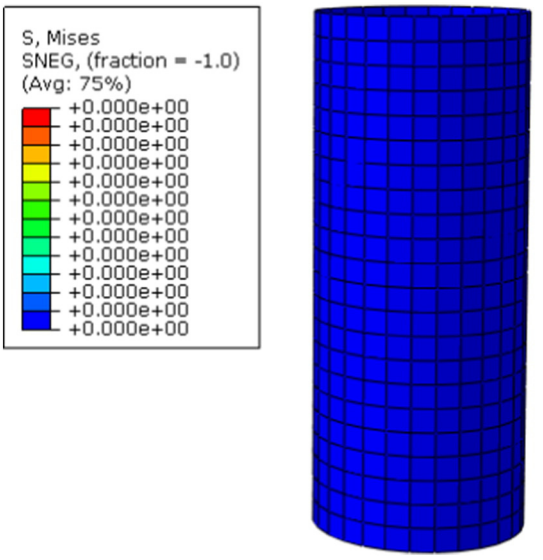


**Fig. 17.** Circular tube model.

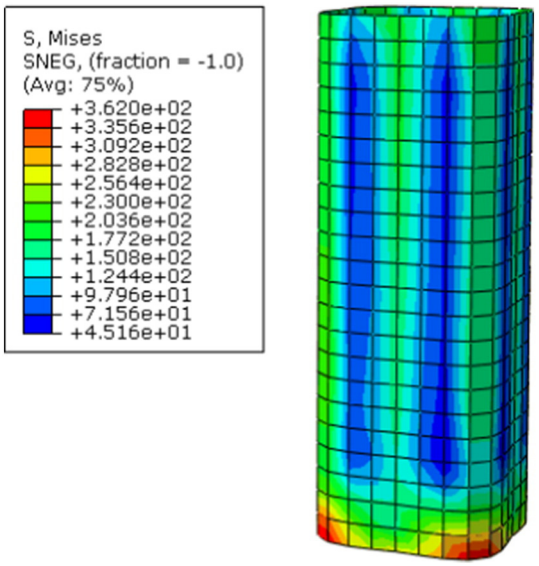


**Fig. 19.** von-Mises stress post-formed (MPa).

The extreme thick-walled cold-formed square steel columns are usually to bear heavily loads, and their height is usually smaller than 8 m, and they are almost worked as stud columns. In this section, the ultimate load under axial compression for a series of columns with different section dimensions ranging from 600 mm × 16 mm to 800 mm × 22 mm and heights ranging from 2.4 m to 8.0 m were analyzed, and the results were list in Table 3.

It is clear from Table 3 that the extreme thick-walled cold-formed square steel columns usually occurred strength failure nor the stability failure, because there has little change for the ultimate load with column height increasing. It is also clear that the ultimate loads obtained from numerical analysis are much smaller than the ultimate loads determined by formula (2) presented in Chinese code (GB 50018-2002) [17], because the formula (2) can not consider the local buckling of steel plate of square columns. In this study, a local buckling adjustment coefficient $\beta$ was introduced to improve the calculation method as shown in formula (3), and the value of $\beta$ was determined as 0.90 based on the data in Table 3. It is clear in Table 3 that the $N_3$ is consistent well with $N_1$ from numerical analysis. Therefore, the formula (3) can be used to predict the ultimate load of the extreme thick-walled cold-formed square steel columns.

$$\frac{N}{\phi A_e} \le \beta f \tag{3}$$

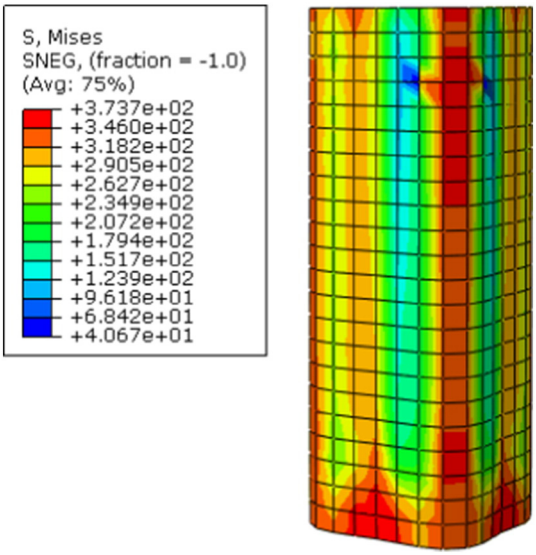


**Fig. 18.** von-Mises stress in forming process (MPa).

## 6. Conclusion

Through the experimental research and numerical analysis of the axial compression behavior of the extremely thick-walled cold-formed square columns, the following conclusions were obtained:

1) The material properties of square cold-formed columns manufactured from circular hollow tube change clearly due to the cold-formed processes; their properties are more uniform than that of cold-formed columns manufactured by steel plates.
2) The main material properties of the extremely thick-walled cold-formed square columns meet the Chinese code requirements. Its yield segment is not clear, and its ductility decreases.
3) The extremely thick-walled cold-formed square columns works well under axial compression, and the average bearing capacity of the two specimens is about 21000kN. A formula was presented in this study to predict the ultimate load of the extreme thick-walled cold-formed square steel columns.

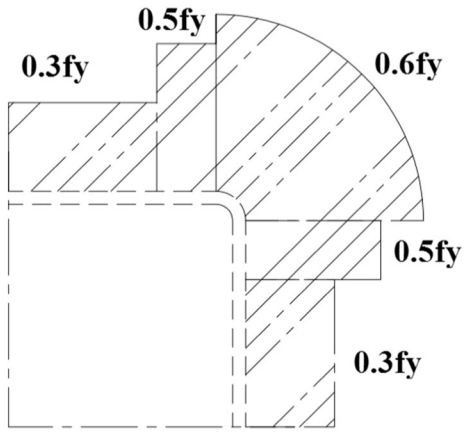


**Fig. 20.** The stress distribution (1/4 section).

**Table 3**
The numerical results and calculation results.

| Specimens(mm) | H(m) | $\varphi$ | $N_1$ (kN) | $N_2$ (kN) | $N_3$ (kN) | $N_1/N_2$ | $N_1/N_3$ |
|---|---|---|---|---|---|---|---|
| 800 × 22 | 2.4 | 0.980 | 19,810 | 22,645 | 20,381 | 0.87 | 0.97 |
| 800 × 22 | 4.8 | 0.960 | 19,500 | 22,184 | 19,966 | 0.88 | 0.98 |
| 800 × 22 | 8.0 | 0.933 | 19,410 | 21,559 | 19,403 | 0.90 | 1.00 |
| 700 × 20 | 2.4 | 0.976 | 17,200 | 19,772 | 17,795 | 0.87 | 0.97 |
| 700 × 20 | 4.8 | 0.936 | 16,940 | 18,962 | 17,066 | 0.89 | 0.99 |
| 700 × 20 | 8.0 | 0.864 | 16,430 | 17,503 | 15,753 | 0.94 | 1.04 |
| 600 × 16 | 2.4 | 0.974 | 12,100 | 13,320 | 11,988 | 0.91 | 1.01 |
| 600 × 16 | 4.8 | 0.925 | 11,690 | 12,648 | 11,383 | 0.92 | 1.03 |
| 600 × 16 | 8.0 | 0.886 | 11,070 | 12,116 | 10,904 | 0.91 | 1.02 |

Note: H stands for the height of steel columns; $N_1$ stands for ultimate load from numerical analysis; $N_2$ stands for ultimate load calculated by formula (2); N3 stands for ultimate load calculated by formula (3).

4) The residual stresses at middle part and corner part of the extremely thick-walled cold-formed square columns manufactured from circular hollow tube are about 95 MPa and 210 MPa, respectively.

## Acknowledgements

This work is sponsored by the National Natural Science Foundation of China (Grant No. 61272264). The authors also appreciate the financial support provided by the Chinese Scholarship Council (File No. 201506255034) that enabled the Visiting Research Scholar to cooperate with Prof. Luke Bisby at University of Edinburgh.

## References

[1] Y.-J. Guo, A.-Z. Zhu, P. Yong-Lin, F. Tin-Loi, Experimental study on compressive strengths of thick-walled cold-formed sections, J. Constr. Steel Res. 63 (5) (2007) 718–723.
[2] T. Lewei, H. Gang, C. Yiyi, Z. Feng, K. Shen, A. Yang, Experimental investigation on longitudinal residual stresses for cold-formed thick-walled square hollow sections, J. Constr. Steel Res. 73 (2012) 105–116.
[3] S. Min, A. Packer Jeffrey, Direct-formed and continuous-formed rectangular hollow sections – Comparison of static properties, J. Constr. Steel Res. 92 (2014) 67–78.
[4] M. Ashraf, L. Gardner, D.A. Nethercot, Strength enhancement of the corner regions of stainless steel cross-sections, J. Constr. Steel Res. 61 (1) (2005) 37–52.
[5] S.-D. Hu, Y. Ben, L. Li-Xin, Materials properties of thick-wall cold-rolled welded tube with a rectangular or square hollow section, Constr. Build. Mater. 25 (2011) 2683–2689.
[6] Q. Wai-Meng, Y. Ben, Material properties of cold-formed and hot-finished elliptical hollow sections, Adv. Struct. Eng. 18 (7) (2015) 1101–1114.
[7] J. Lu, L. Hongbo, C. Zhihua, X. Liao, Experimental investigation into the post-fire mechanical properties of hot-rolled and cold-formed steels, J. Constr. Steel Res. 121 (2016) 291–310.
[8] L. Gardner, N. Saari, F. Wang, Comparative experimental study of hot-rolled and cold-formed rectangular hollow sections, Thin-Walled Struct. 48 (2010) 495–507.
[9] W.W. Yu, Cold-Formed Steel Design. 3rd, John Wiley and Sons, New York, 2000.
[10] G.J. Hancock, Design of Cold-Formed Steel Structures, 3rd ed Sydney, Australian Institute of Steel Construction, 1998.
[11] Y. Ben, L. Ya-hua, Experimental investigation of cold-formed stainless steel columns, J. Struct. Eng. ASCE 129 (2) (2003) 169–176.
[12] C. Tak-Ming, Z. Xiao-Ling, Y. Ben, Cross-section classification for cold-formed and built-up high strength carbon and stainless steel tubes under compression, J. Constr. Steel Res. 106 (2015) 289–295.
[13] O. Zhao, G. Leroy, Y. Ben, Structural performance of stainless steel circular hollow sections under combined axial load and bending-part 1: Experiments and numerical modeling, Thin-Walled Struct. 101 (2016) 231–239.
[14] L. Yuan-qi, L. Gong-wen, S. Zu-yan, et al., Modification method for yield strength ofcold-formed thick-walled steel sections considering cold-forming effect, J. Build. Struct. 36 (5) (2015) 1–7 (in Chinese).
[15] L. Li-ming, J. Xin-liang, C. Zhi-hua, et al., Strain hardening of thick-walled cold formed steeltube, J. Tianjin Univ. 41 (1) (2008) 85–91 (in Chinese).
[16] GB/T 228-2010, Metallic Material-Tensile Testing Part 1: Method of Test at Room Temperature, Standard Press of China, 2010 (in Chinese).
[17] GB 50018-2002, Technical Code of Cold-Formed Thin-Walled Steel Structures, Standards Press of China, 2002 (in Chinese).